water

MDPI

Article

Hydrochemical Characteristics and Formation Mechanism of Quaternary Groundwater in Baoshan Basin, Western Yunnan, China

Yi Xiao [1,2], Jiahui Zhang [3,*], Aihua Long [1,2,*], Shiguang Xu [4], Tingting Guo [3], Xinchen Gu [2,5], Xiaoya Deng [2] and Pei Zhang [2]

[1] College of Water Conservancy & Architectural Engineering, Shihezi University, Shihezi 832000, China; yam273021691@163.com
[2] State Key Laboratory of Simulation and Regulation of Water Cycle in River Basin, China Institute of Water Resources and Hydropower Research, Beijing 100044, China
[3] Department of Earth Sciences, Kunming University of Science and Technology, Kunming 650093, China
[4] Yunnan Geological and Mineral Engineering Survey Group Company, Kunming 650000, China
[5] State Key Laboratory of Hydraulic Engineering Simulation and Safety, School of Civil Engineering, Tianjin University, Tianjin 300072, China
* Correspondence: jiahuizhang2307@163.com (J.Z.); ahlong@iwhr.com (A.L.)

Abstract: The shallow groundwater of the quaternary system in the Baoshan basin, Yunnan Province is seriously polluted, threatening human health and restricting local socio-economic development; therefore, it is necessary to investigate the hydrochemical characteristics and formation mechanisms of the shallow groundwater of the quaternary system in the Baoshan basin. This study used EVS 2022 to establish a 3D visual geological model of the quaternary system in the basin and divided the shallow groundwater aquifers of the quaternary system into three groundwater systems, sampling 22, 9, and 4 groups in each groundwater system, respectively. Mathematical statistics, Piper's trilinear diagram, Gibbs plots, the Gaillardet model, the ion ratio method, groundwater saturation, and the PCA-APCS-MLR model were used to analyze the groundwater hydrochemical characteristics and genesis of the study area. The results show the following: (1) The types of groundwater chemicals are mainly HCO_3-Ca-Mg type and HCO_3-Ca, the causes of the water chemical characteristics are mainly influenced by water–rock interaction and alternate cation adsorption, and the rock types with which the groundwater exchanges substances are carbonate rocks and silicate rocks. (2) The Fe^{2+}, Mn^{2+}, and NH_3-N contents in groundwater systems I and II exceed the standard, which is the human activity area, and groundwater pollution is mainly affected by human activities. (3) Four main categories of factors were obtained according to the PCA-APCS-MLR model, namely dissolution filtration, migration and enrichment factors, geological and human activity factors, and environmental factors and pollution factors; the cumulative contribution of variance was 77.84%, and the groundwater chemical characteristics were jointly influenced by hydrogeological conditions and human activities. The results of this study provide a basis for groundwater protection and management in the Baoshan basin, where groundwater system I is the key area for pollution and should be strengthened for control.

Keywords: quaternary shallow groundwater; hydrochemical characteristics; water pollution; PCA-APCS-MLR model; Baoshan basin

Citation: Xiao, Y.; Zhang, J.; Long, A.; Xu, S.; Guo, T.; Gu, X.; Deng, X.; Zhang, P. Hydrochemical Characteristics and Formation Mechanism of Quaternary Groundwater in Baoshan Basin, Western Yunnan, China. *Water* **2023**, *15*, 2736. https://doi.org/10.3390/w15152736

Academic Editors: Paolo Madonia and Cesar Andrade

Received: 10 June 2023
Revised: 8 July 2023
Accepted: 25 July 2023
Published: 28 July 2023

1. Introduction

Groundwater has the characteristics of wide distribution, stable changes, good water quality, and easy application, making it an important resource indispensable for the long-term and stable development of human beings on Earth [1]. The current demand for groundwater resources has increased greatly, and unreasonable exploitation has caused the deterioration of groundwater quality. Probing its groundwater chemical characteristics

and causes can provide an important guarantee for groundwater quality monitoring and the sustainable development of socio-economic, industrial, agricultural, and ecological health [2–4].

Groundwater chemistry components are changing every moment due to the fact that groundwater exchanges substances with the external environment through flow, and the formation and evolution of groundwater during the water cycle are influenced by natural factors such as water–rock interaction [5–7], evaporation concentration [8–10], ion exchange [11,12], and redox [13]. Many scholars at home and abroad have conducted various studies on groundwater chemical characteristics and hydrochemical causes; the main research methods include statistical analysis [14,15], graphical methods [16,17], and ion proportionality [18,19], and the related research results are becoming increasingly fruitful. The impact of human activities such as industrialization and urbanization on groundwater is increasing [20,21], and many scholars have carried out risk assessment, pollution source identification, and wastewater treatment for heavy metals and organic matter contamination in groundwater [22]. However, traditional methods of water chemistry analysis encounter difficulty in quantitatively describing the complex evolution of groundwater chemistry under the conditions of human activities, and multivariate statistical models currently provide a more accurate and convenient method of groundwater chemistry characterization and pollution cause analysis [23,24].

The Baoshan basin is a typical quaternary fault basin in western Yunnan province, and quaternary groundwater is an important water supply source for resource production and the life of residents in the basin; however, groundwater indicators such as iron, manganese, and ammonia nitrogen seriously exceed the standard levels, which greatly threatens the productiveness of the region and safety of local people [25]. In order to ensure the long-term and stable utilization of quaternary groundwater resources in the Baoshan basin, it is urgent to understand the chemical characteristics of this groundwater and analyze the causes of pollution; however, few studies in this area have been reported in recent years. In this paper, we combine traditional hydrogeochemical methods and multivariate statistical methods to describe in detail the statistical characteristics of chemical indicators and groundwater chemical types in the quaternary groundwater of the Baoshan basin, determine the sources of groundwater ionic components, and analyze the causes of groundwater pollution, with the aim of providing a scientific basis for groundwater development, utilization, management, and protection in the Baoshan basin.

2. Materials and Methods

2.1. Study Area

The Baoshan basin in western Yunnan, with geographic coordinates of 98°08′ to 99°16′ E and 24°56′ to 25°14′ N, is located at the junction of China and Myanmar. The Baoshan basin is a lacustrine plain landscape surrounded by mountains and hills; the basin is oriented in the north–south direction [26] and is 15 km long and 7–10 km wide, with a total area of 230 km^2 (Figure 1). The Baoshan basin is located at low latitudes and high altitudes, with an average annual temperature of 14.7 °C. The average annual rainfall in Baoshan is about 1047.3 mm and the average annual evaporation is 1650.3 mm [27]. There are many rivers in the Baoshan basin, with the Donghe River being the main water system in the basin, flowing from the northern part of the basin; its tributaries on the east and west sides converge into the main river channel and then run off from north to south, finally discharging to the Nujiang River. The main stream of the Donghe River is 25.3 km long in the basin, which is the lowest erosion datum in the region.

The Baoshan basin is covered by quaternary sediments, and the surface outcrops are the quaternary holocene and quaternary pleistocene. The quaternary holocene sediments are mainly lacustrine deposits, which are gray and brown clay and pebble gravel layers mainly distributed in the center of the Baoshan basin and with a maximum thickness of 35.84 m [28,29]. Atmospheric precipitation is the main recharge term for groundwater in this formation. In addition, agriculture and industry are mostly concentrated in the central part

of the Baoshan basin, and agricultural irrigation water and domestic wastewater infiltrate into the aquifer in a facultative form. Due to the large hydraulic gradient, the bedrock fracture water and carbonate rocks in the surrounding mountains recharge the central part of the basin, and when the rainfall is high the river level rises rapidly, which locally causes the river to backcharge the groundwater [30]. The quaternary pleistocene consists of river and lake phase sediment of river alluvium, including clay, red clay, and gravel layers, which are mainly distributed at the edge of the Baoshan basin. The main source of groundwater recharge in this formation is atmospheric precipitation, and it is in contact with karst aquifers in the southern and northeastern part of the bedrock mountains; groundwater receives recharge from karst water and fissure water in the mountains. Groundwater in the region mainly runs toward the middle of the basin with a slow seepage rate, and eventually discharges to the Donghe River [28,29]. The surrounding mountainous areas are dominated by sedimentary clastic and carbonate rocks, and the main lithologies include limestones, argillaceous limestones, shales, and sandstones.

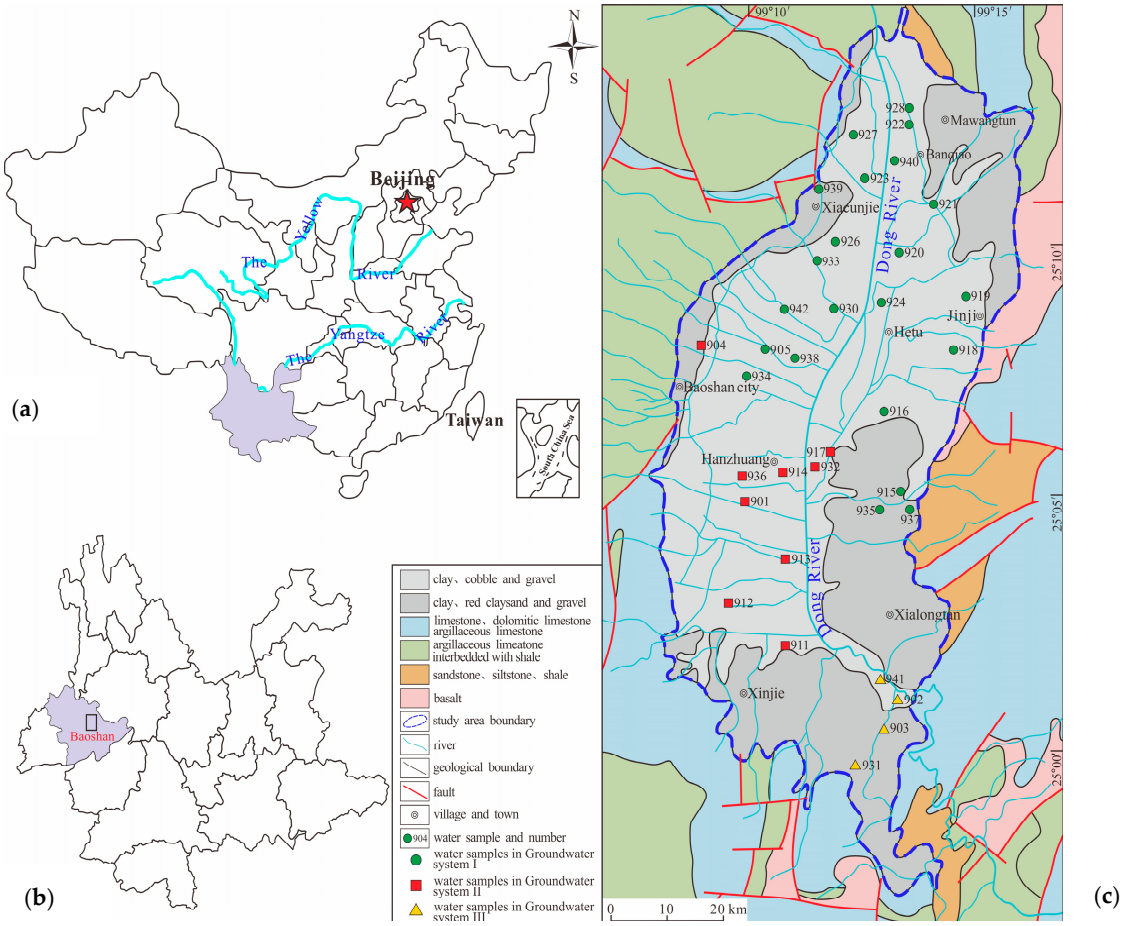

Figure 1. Distribution of regional hydrogeology and groundwater sampling points in the Baoshan basin, SW China: (**a**) location of Yunnan Province; (**b**) location of Baoshan basin; (**c**) regional hydrogeology of the Baoshan basin. The green points are the water samples in groundwater system I, the red points are the water samples in groundwater system II, and the yellow points are the water samples in groundwater system III.

2.2. Groundwater System

By collecting engineering geological borehole data, the quaternary strata in the basin can be generalized into seven layers according to the nature and water-richness of the geotechnical body: plain fill, clay, cobble and gravel, clay, sand and gravel, clay, and red clay. The 3D geological modeling software Earth Volumetric Studio (EVS) [31] was used to

establish a 3D geological model of the quaternary system in the Baoshan basin (Figure 2a) in order to visualize and analyze the quaternary strata in the Baoshan basin visually and clearly and then delineate the groundwater system, providing a basis for groundwater chemical characterization.

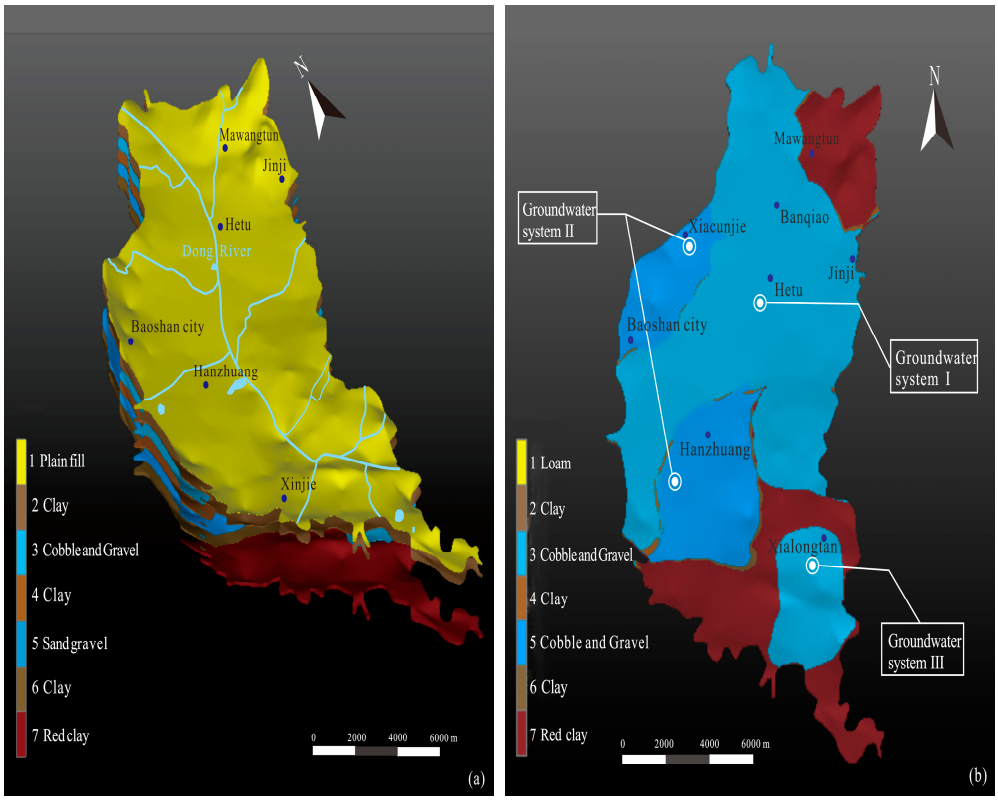

Figure 2. Three-dimensional geological model of quaternary system in Baoshan basin: (**a**) stratigraphic structure and (**b**) groundwater systems.

According to the hydrogeological conditions in the region, the Baoshan basin was divided into three groundwater systems, namely, groundwater system I, groundwater system II, and groundwater system III (Figure 2b).

2.3. Sample Collection and Testing

The groundwater samples were collected from residential wells and agricultural irrigation wells in 2019, and the sampling depths ranged from 0 to 20 m. The samples were all shallow groundwater. The groundwater system was used as the unit, with 22 groups of groundwater system I (green points in Figure 1c), 9 groups of groundwater system II (red points in Figure 1c), and 4 groups of groundwater system III (yellow points in Figure 1c), totaling 35 groups; the sampling points were labeled according to the sampling order.

A total of 28 indicators were selected for the water chemistry test, including pH, TDS, TH, seven major ions, organic substances, inorganic substances, and heavy metals. pH was measured on site using a PHS-3C pH meter, and the rest of the indicators in the groundwater samples were measured in the laboratory of Yunnan Sino-sci Testing Tech. Co, Ltd. (Shenzhen, China), HCO_3^-, Cl^-, and SO_4^{2-} were determined by acidity titration, the silver nitrate volumetric method, and the barium sulfate turbidimetric method, respectively; Ca^{2+} and Mg^{2+} were determined using the ASS method; Na^+, K^+, Fe^{2+}, and Mn^{2+} were determined via the FAAS method; and TDS, TH, COD, and NH_3-N were determined using the weighing method, EDTA method, CODMn method, and nano-reagent photometric method, respectively.

To ensure the reliability of the data, the anion and cation balance reliability test was performed on all the test results; the results showed that the relative error of anion and

cation balance for all the water samples was between ±6% and that the test results were reliable. In this paper, ArcGIS 10.2, EVS 2022, Origin2021, PHREEQC 3.7.3, and SPSS 27 were used for water chemistry characterization, and the PCA-APCS-MLR model was used for groundwater pollution source analysis using SPSS software.

3. Results

3.1. Hydrochemical Characteristics

SPSS software was used to analyze 35 sets of water samples within the Baoshan basin and to count the parameter characteristic values of the water chemistry conventional components of the groundwater samples collected (Figure 3 and Table 1). The mean values reflect the overall situation of each conventional ion concentration index in the whole study area. The mean values of the cation concentration in each groundwater system of the shallow quaternary groundwater in the Baoshan basin are in the order of $Ca^{2+} > Na^{+} > Mg^{2+} > K^{+}$ from high to low, and Ca^{2+} is the most abundant cation in the shallow groundwater of the basin. The average values of anion concentrations from high to low are $HCO_3^{-} > Cl^{-} > SO_4^{2-}$, and HCO_3^{-} is the most abundant anion in the groundwater of the basin. For the three groundwater systems described separately, the TDS concentration values were in the range of 186.00–617.00 mg/L, 230.00–751.00 mg/L, and 247.00–320.00 mg/L, with mean values of 343.20 mg/L, 484.56 mg/L, and 293.73 mg/L, over all freshwater (TDS < 1000 mg/L). The TH concentration values were in the range of 117.00–446.00 mg/L, 135.00–442.00 mg/L, and 159.00–379.00 mg/L, with mean values of 278.86 mg/L, 278.00 mg/L, and 291.00 mg/L. One group of hard water (300 mg/L < TH < 450 mg/L) was found in each of groundwater system I and groundwater system II, while the rest were slightly hard water (150 mg/L < TH < 300 mg/L).

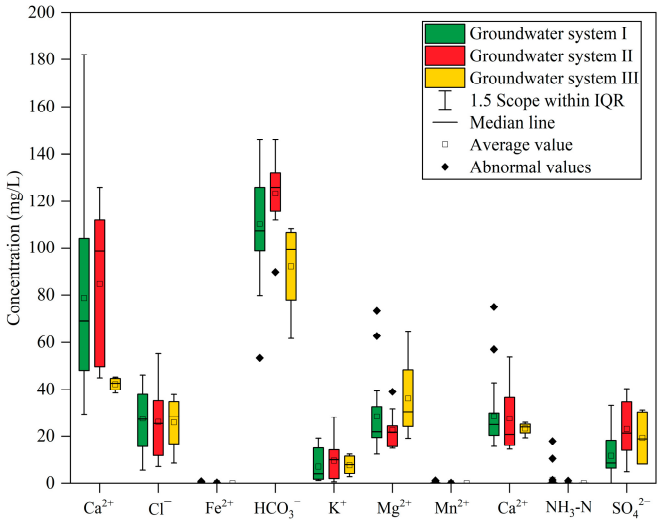

Figure 3. Box diagram of groundwater chemical composition in Baoshan basin.

The coefficient of variation was mainly used to compare the relationship between statistical indicators; a smaller coefficient of variation indicates that the variability of the variables is not significant, and a larger number of variances indicates that the chemical components of groundwater underwent a complex evolutionary process during its formation and evolution [32]. The pH intervals of the three groundwater systems were 6.17–8.27 mg/L, 7.22–8.29 mg/L, and 7.63–8.17 mg/L, with mean values of 7.81 mg/L, 7.96 mg/L, and 7.83 mg/L, respectively. The coefficients of variation were 0.07, 0.05, and 0.03, indicating that the spatial variability of the pH was not significant, and the groundwater was weakly alkaline in general. The coefficients of variation of Ca^{2+}, Mg^{2+}, Na^{+}, HCO_3^{-}, and Cl^{-} ranged from 0.19 to 0.52, indicating that the distribution of the above ions was relatively stable in each groundwater system. The SO_4^{2-} concentration ranges were 0.00–33.22 mg/L, 5.10–40.40 mg/L, and 8.30–31.20 mg/L, with mean values of 11.66 mg/L,

22.98 mg/L, and 19.30 mg/L, respectively. The coefficient of variation was 0.90 in groundwater system I, 0.53 and 0.66 in groundwater system II and III, and the concentrations at water sample points 901 and 913 were 40.4 mg/L and 35.1 mg/L, respectively, which were more than twice the average value. It was speculated that the local ultra-high value of SO_4^{2-} in groundwater system I might be related to mixing with hot spring water. The K^+ concentration ranges were 1.11–19.20 mg/L, 0.58–28.00 mg/L, and 2.73–12.40 mg/L, with mean values of 7.22 mg/L, 9.65 mg/L, and 7.81 mg/L, respectively, in the groundwater systems. The coefficients of variation were 0.92 and 0.94 in groundwater systems I and II, respectively, and 0.58 in groundwater system III. The concentrations at water sample points 913, 921, and 922 were 28.00 mg/L, 18.50 mg/L, and 19.20 mg/L, respectively, indicating that K^+ is unevenly distributed in groundwater concentration values and is a sensitive factor susceptible to the groundwater environment and the local location of K^+. The very high value of K^+ may be closely related to local agricultural production. The coefficients of variation of Fe^{2+}, Mn^{2+}, and NH_3-N were greater than in groundwater systems I and II, and the coefficient of variation of COD was greater than in groundwater system I. In groundwater system III, Fe^{2+} and Mn^{2+} were not detected, and the coefficients of variation of NH_3-N and COD were 0.23 and 0.22, respectively; the above four indicators had obvious spatial variation, and represent the main pollutants in the groundwater of the Baoshan basin.

Table 1. Statistical results of the groundwater chemical parameters.

Indicators	Groundwater System I (*n* = 22)				Groundwater System II (*n* = 9)				Groundwater System III (*n* = 4)			
	Min	Max	Mean	Cv	Min	Max	Mean	Cv	Min	Max	Mean	Cv
pH	6.17	8.27	7.81	0.07	7.22	8.29	7.96	0.05	7.63	8.17	7.83	0.03
TDS	186.00	617.00	343.20	0.38	230.00	751.00	484.56	0.38	247.00	320.00	293.75	0.12
TH	117.00	446.00	278.86	0.32	135.00	442.00	278.00	0.41	159.00	379.00	291.00	0.33
Na^+	15.70	75.00	28.40	0.49	14.50	54.00	27.46	0.51	19.30	25.80	23.18	0.12
K^+	1.11	19.20	7.22	0.92	0.58	28.00	9.65	0.94	2.73	12.40	7.81	0.58
Ca^{2+}	29.30	182.00	78.79	0.46	45.00	126.00	84.67	0.37	38.60	45.30	42.33	0.07
Mg^{2+}	12.40	73.30	28.34	0.53	14.90	39.10	22.53	0.37	19.10	64.70	36.15	0.55
Cl^-	5.80	46.10	27.39	0.42	7.30	55.40	25.96	0.61	8.70	37.90	25.73	0.49
SO_4^{2-}	0.00	33.22	11.66	0.90	5.10	40.40	22.98	0.53	8.30	31.20	19.30	0.66
HCO_3^-	55.59	146.00	110.06	0.19	89.80	146.00	123.39	0.13	61.70	108.00	92.18	0.23
NH_3-N	0.00	1.40	0.15	2.55	0.00	19.90	2.62	2.48	0.00	0.70	0.23	1.47
Fe^{2+}	0.00	0.78	0.07	2.83	0.00	0.26	0.03	3.00	0.00	0.00	/	/
Mn^{2+}	0.00	1.14	0.15	2.12	0.00	0.17	0.02	2.66	0.00	0.00	/	/
COD	0.35	6.53	1.44	1.09	0.51	1.34	0.80	0.37	0.46	0.74	0.56	0.22

Notes: pH is dimensionless, the rest of the units are mg/L; "/" means there is no such calculation result.

By analyzing the relationship between the ratio of the molarity of ions to the molarity of the total dissolved ions and TDS, the contribution of the major ionic components to TDS in groundwater can be obtained (Figure 4). The contribution of HCO_3^- to TDS ranges from 19.8% to 60.8%; the contribution of Ca^{2+} to TDS ranges from 11.5% to 37.4%; and the contribution of Na^+ to TDS ranges from 4.9% to 19.8%. The anion with the highest contribution to TDS in all three groundwater systems was HCO_3^-, and the cations with high contribution were Ca^{2+} and Na^+. This shows that the highest content of HCO_3^-, Ca^{2+}, and Na^+ in the groundwater of the study area is consistent with the results of the statistical characteristic value analysis of water chemistry parameters.

3.2. Hydrochemical Types

The Piper trilinear diagram can reflect the main anions and cations in groundwater and their concentration ratios, and provides a classification basis for analyzing groundwater chemical types [33], which plays a very important role in revealing hydrogeochemical laws. According to the analysis of the Piper diagram (Figure 5), the water sample points mainly fall in the 1/3/5 zone of the Piper diagram, indicating that the mass concentra-

tions of alkaline earth metal ions in the samples all exceed the mass concentrations of alkali metal ions. Ca^{2+} was the dominant cation in the study area, with concentrations ranging from 25.16% to 70.81% milligram equivalent percent, followed by Mg^{2+} and Na^{+}, with concentrations ranging from 15.9% to 61.29% and 8.48% to 36.12% milligram equivalent percent, respectively. HCO_3^{-}, a weak acid ion, is the core anion in the study area, with the concentration of this ion ranging from 37.05% to 93.6% milligram equivalent percent, followed by Cl^{-}, with concentrations ranging from 6.4% to 46.11% milligram equivalent percent.

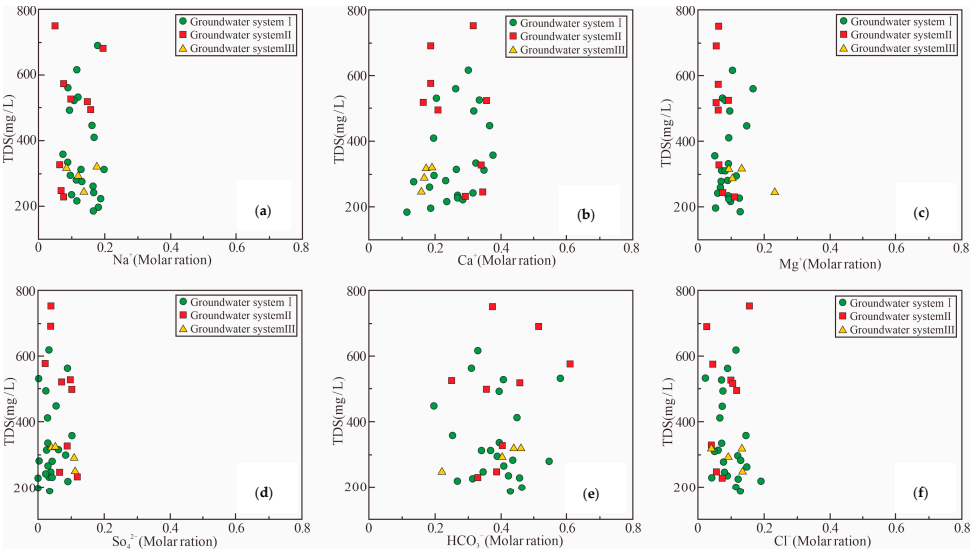

Figure 4. Contribution of major ions to TDS in groundwater: (**a**) contribution of Na^{+} to TDS; (**b**) contribution of Ca^{2+} to TDS; (**c**) contribution of Mg^{2+} to TDS; (**d**) contribution of SO_4^{2-} to TDS; (**e**) contribution of HCO_3^{-} to TDS; (**f**) contribution of Cl^{-} to TDS.

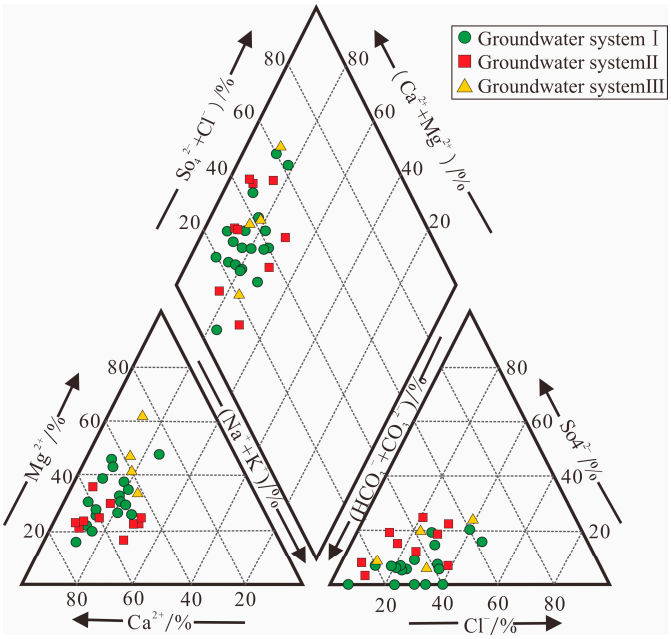

Figure 5. The Piper trilinear diagram for the groundwater samples.

The hydrochemical types in the study area include HCO_3-Ca, HCO_3-Ca-Na type, HCO_3-Ca-Mg type, HCO_3-Cl^{-}Ca type, Cl^{-}Ca type, HCO_3-Cl^{-}Ca-Na type, and HCO_3-Cl^{-}Ca-Mg type. The groundwater chemistry types at the groundwater sample sites in

groundwater system III were all HCO_3-Ca-Mg types. Each hydrochemical type was distributed in groundwater system I and groundwater system II, and the HCO_3-Ca-Mg and HCO_3-Ca types were the main groundwater chemistry types in the study area.

Total salinity (TIS) is another important indicator used to characterize groundwater chemistry; it characterizes the sum of the concentrations of the major anions and cations. The major anions (SO_4^{2-} and HCO_3^-+Cl^-) in the water samples were selected as characteristic values [34] and the isosalinity contours were plotted (Figure 6). The water sample points of groundwater system I were distributed between 7 and 16 meq·L^{-1} salinity contours, the water sample points of groundwater system II were distributed between 9 and 16 meq·L^{-1} salinity contours, and the water sample points of groundwater system III were distributed between 7 and 11 salinity contours. The milligram equivalent concentration of SO_4^{2-} at each water sample site was less than 0.50 meq·L^{-1}, while the milligram equivalent concentration of HCO_3^-+Cl^- was greater than 1.75 meq·L^{-1}, indicating that the main anions in the groundwater of the Baoshan basin were HCO_3^-. Among the individual groundwaters, the groundwater of groundwater system II had the highest percentage of HCO_3^-+Cl^- while groundwater system III had the least.

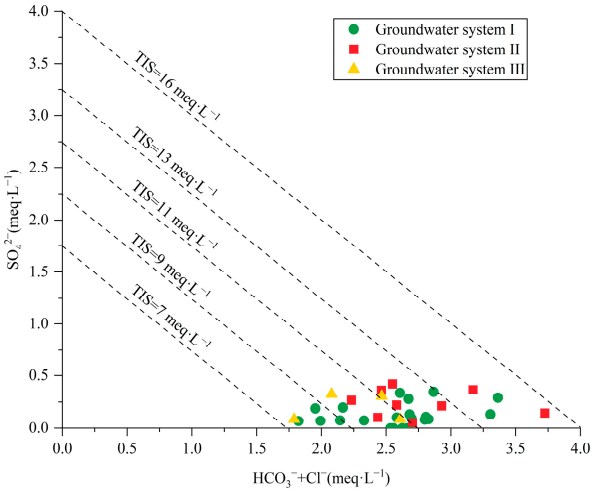

Figure 6. Correlation diagram of SO_4^{2-} and HCO_3^-+Cl^-.

3.3. Natural Sources of Groundwater Ion Fractions

3.3.1. Gibbs Plots

Gibbs plots can directly reflect the constraints and formation system of the main ions in the water column, including water–rock interaction, evaporation, and rainfall, which can lead to changes in the chemical composition of the groundwater column and changes in TDS [35].

The TDS values of the shallow groundwater of the quaternary system in the Baoshan basin ranged from 186 mg/L to 751 mg/L, $Na^+/(Na^+{+}Ca^{2+})$ from 0.12 to 0.52, and $Cl^-/(Cl^-{+}HCO_3^-)$ from 0.04 to 0.42. The groundwater sample points of the three groundwater systems were mostly scattered in the area where the $Na^+/(Na^+{+}Ca^{2+})$ and $Cl^-/(Cl^-{+}HCO_3^-)$ were less than 0.5 in the horizontal coordinate (Figure 7). The anions and cations in the groundwater mainly originated from the material exchange between the groundwater and the surrounding rock layers. The $Na^+/(Na^+{+}Ca^{2+})$ of individual water sample points in groundwater system I was greater than 0.5 and the water sample points were shifted to the upper right region, indicating that the groundwater at these water sample points is buried at a shallow depth and is affected by evaporation to an extent.

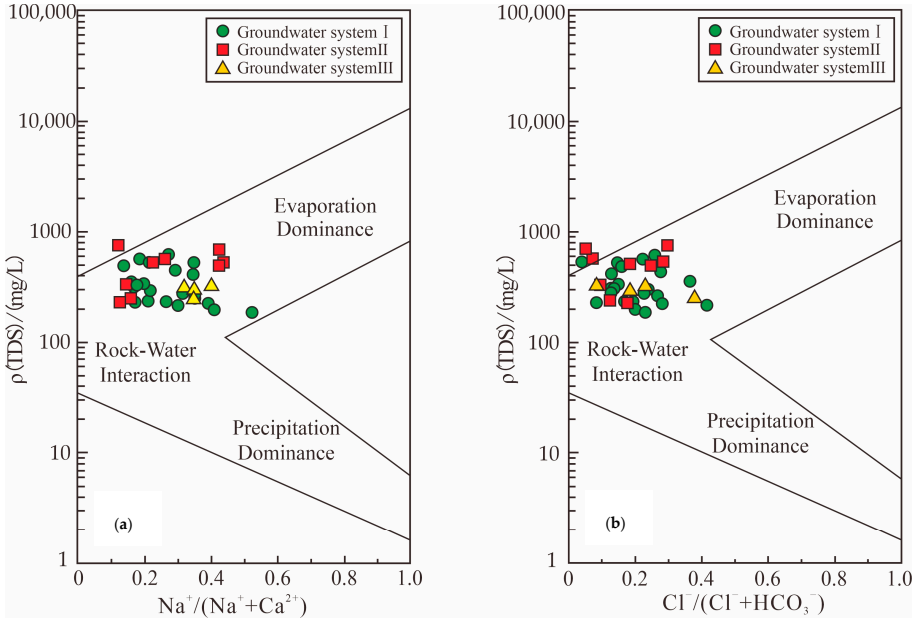

Figure 7. Gibbs plots of groundwater: (**a**) relationship between $Na^+/(Na^+ + Ca^{2+})$ and TDS and (**b**) relationship between $Cl^-/(Cl^- + HCO_3^-)$.

3.3.2. Dissolved Filtration of Rocks

The Gibbs plots allow a preliminary judgment to be made: the hydrochemical genesis of groundwater in the study area is closely related to water–rock interaction. To illustrate the specific water–rock interaction process, the Gaillardet model needs to be invoked for a further explanation of the water–rock process [36]. The model has three different units of water–rock interaction along the diagonal of the rectangle from the lower left to the upper right corner for evaporite, silicate, and carbonate rocks, in that order. The ratio of HCO_3^-/Na^+ to Ca^{2+}/Na^+ is calculated, and the position of this value in the model is the type of water–rock interaction. The Gaillardet model was established based on the test data of groundwater samples taken from the study area (Figure 8), from which it can be seen that the groundwater sample points in the study area are mainly located in the action interval of silicate and carbonate rocks, and far from the evaporite action interval. Combined with the types of geotechnical bodies in and around the basin, a preliminary conclusion can be drawn that the formation of groundwater chemical characteristics in the basin is mainly related to the dissolution and filtration of carbonate rocks and silicate rocks.

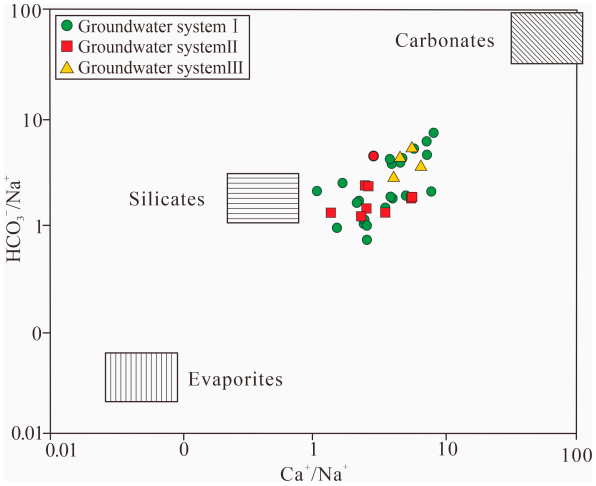

Figure 8. Gaillardet diagram based on the relationship between Ca^{2+}/Na^+ and HCO_3^-/Na^+.

3.3.3. Ion Proportionality Coefficient Characteristics

Through the Gaillardet model analysis, only the types of rocks that exchange material with groundwater in the basin can be known as carbonate rocks and silicate rocks. However, it is not possible to analyze which rock types exchange material with groundwater more strongly; thus, the ionic proportion coefficient method is needed in order to make any further judgment [37].

The ratio of Na^+ and Cl^- concentrations is called the groundwater genesis factor, a hydrogeochemical parameter characterizing the degree of Na^+ enrichment in groundwater [37]. If the value of Na^+/Cl^- in groundwater is close to 1, this indicates that Na^+ and Cl^- in groundwater mainly originate from the atmospheric precipitation or dissolution of rock salt; if the value is >1, this indicates that Na^+ and Cl^- may originate from cation exchange [37]. The Na^+/Cl^- ion ratio coefficient relationship (Figure 9) shows that most groundwater samples have a good correlation between sodium and chloride ions. There are 85.8% of groundwater sampling points with $Na^+/Cl^- > 1$, indicating that Na^+ and Cl^- are mainly subject to alternate cation adsorption. A total of 14.2% of groundwater sampling points with $Na^+/Cl^- < 1$ confirm that the source of Cl^- is not unique and that the possibility of groundwater contamination by human activities (domestic sewage and livestock manure effluent) is extremely high.

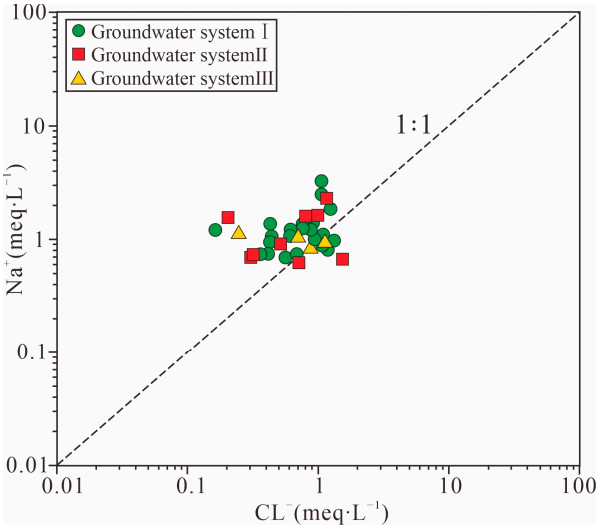

Figure 9. Relationship between Na^+ and Cl^-.

The contribution of the dissolution of other rock types to groundwater chemistry can be judged by the relationship of the ratio coefficient of $(Ca^{2+}+Mg^{2+})/(SO_4{}^{2-}+HCO_3{}^-)$. When the sample points are located above the 1:1 line, $Ca^{2+}+Mg^{2+}$ is more than $SO_4{}^{2-}+HCO_3{}^-$, implying that the water–rock interaction is dominated by the dissolution of carbonate rocks. When the sample points are located below the 1:1 line, this indicates that the water–rock interaction is dominated by weathering dissolution of silicate rocks. The groundwater sample points in all three groundwater systems are located above the 1:1 line (Figure 10), indicating that carbonate rocks are the main factors controlling the sources of Ca^{2+}, Mg^{2+}, $SO_4{}^{2-}$, and $HCO_3{}^-$ in groundwater in the Baoshan basin. The dissolved amount of carbonate rocks in groundwater system I and groundwater system III is greater than that in groundwater system II.

According to the $(Cl^-+SO_4{}^{2-})/HCO_3{}^-$ ratio coefficient relationship (Figure 11), the water sample points in groundwater system III are all located below the 1:1 line, indicating that the groundwater components in this system mainly originate from carbonate rock dissolution in the mountains around the basin. Most of the water sample points in groundwater system I and groundwater system II are located below the 1:1 line, indicating that the groundwater components in the system mainly originate from carbonate rock dissolution. A small number of water sample points near Hanzhuang are located above the 1:1 line,

which is due to the poor runoff conditions in the area, which mainly dissolve materials in the loose quaternary rock layers. In general, most of the groundwater sample points in the study area are distributed below the 1:1 line and a small number of water sample points are distributed below the 1:1 line, indicating that the dissolution of carbonate rocks dominates in the groundwater of the study area.

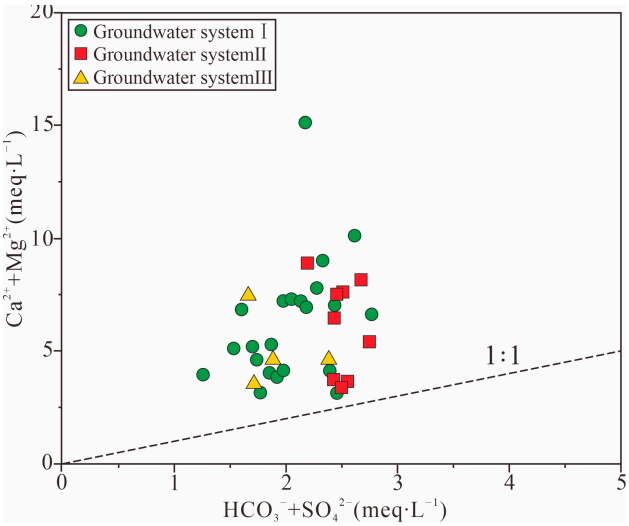

Figure 10. Relationship between ($Ca^{2+}+Mg^{2+}$) and ($SO_4^{2-}+HCO_3^-$).

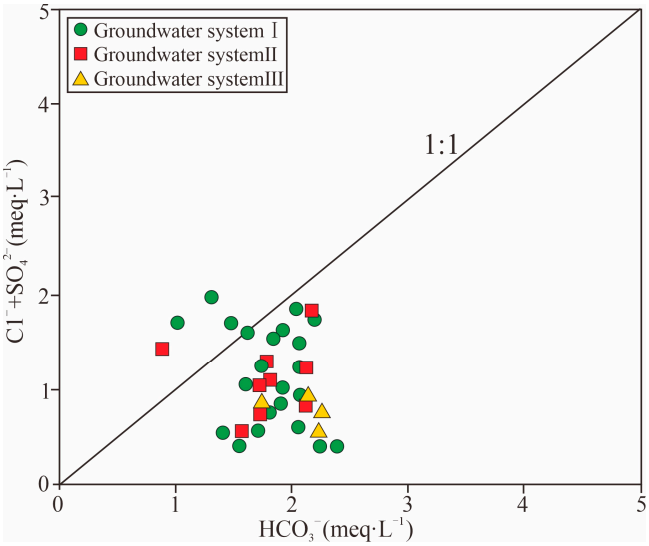

Figure 11. Relationship between ($Cl^-+SO_4^{2-}$) and HCO_3^-.

The cations in groundwater in the basin alternatively adsorb with the cations in the rock and soil bodies on the runoff pathway during the runoff process. The dissolution of atmospheric CO_2 in groundwater, which results in the production of HCO_3^- in groundwater, accelerates the dissolution rate of carbonate rocks following the following chemical equation:

$$CaCO_3+CO_2+H_2O \rightleftharpoons Ca^{2+}+2HCO_3^- \quad (1)$$

$$MgCO_3+CO_2+H_2O \rightleftharpoons Mg^{2+}+2HCO_3^- \quad (2)$$

$$CaMg(CO_3)_2+CO_2+H_2O \rightleftharpoons Ca^{2+}+Mg^{2+}+4HCO_3^- \quad (3)$$

The dissolution of limestones and argillaceous limestones leads to higher Ca^{2+} and Mg^{2+} concentrations in groundwater. The low mineralization of groundwater in the basin provides favorable conditions for the alternating cation adsorption of Ca^{2+} and Mg^{2+} in groundwater, with Na^+ and K^+ attached to the surface of rock and soil bodies. However, as the concentration of Na^+ and K^+ in groundwater increases, it may cause a reverse reaction. In this study, the chloride and alkali index was selected to analyze the specific exchange process of groundwater in the basin [38].

$$CAI1 = Cl^- - \left(Na^+ + K^+\right)/Cl^- \tag{4}$$

$$CAI2 = Cl^- - \left(Na^+ + K^+\right)/SO_4^{2-} + HCO_3^- + NO_3^- + CO_3^{2-} \tag{5}$$

The exchange of cations in groundwater can be divided in two ways: forward exchange and reverse exchange.

The positive cation exchange effect is

$$\begin{aligned}(Ca^{2+}\text{or } Mg^{2+})(\text{rock}) + 2Na^+(\text{groundwater}) \\ \rightarrow 2Na^+\text{rock} + (Ca^{2+}\text{or } Mg^{2+})(\text{groundwater})\end{aligned} \tag{6}$$

The reverse cation exchange interaction is

$$\begin{aligned}2Na^+\text{rock} + (Ca^{2+}\text{or } Mg^{2+})(\text{groundwater}) \\ \rightarrow (Ca^{2+}\text{or } Mg^{2+})(\text{rock}) + 2Na^+(\text{groundwater})\end{aligned} \tag{7}$$

According to the chlor-alkali index in the study area (Figure 12), the vast majority of water sample points in groundwater system III fall into the CAI1 < 0 and CAI2 < 0 regions, indicating that reverse exchange occurs in this groundwater system and that the Ca^{2+} and Mg^{2+} contents in groundwater are reduced. Most of the water sample points in groundwater system I and groundwater system II fall in the area of CAI1 < 0 and CAI2 < 0. Only in the area around Hanzhuang do the water sample points fall into the area of CAI1 > 0 and CAI2 > 0, indicating that the Ca^{2+} and Mg^{2+} contents are high in most areas of the two groundwater systems and that it is easy for reverse exchange to occur. In the area of Hanzhuang, positive exchange occurs due to the low Ca^{2+} and Mg^{2+} contents in the groundwater.

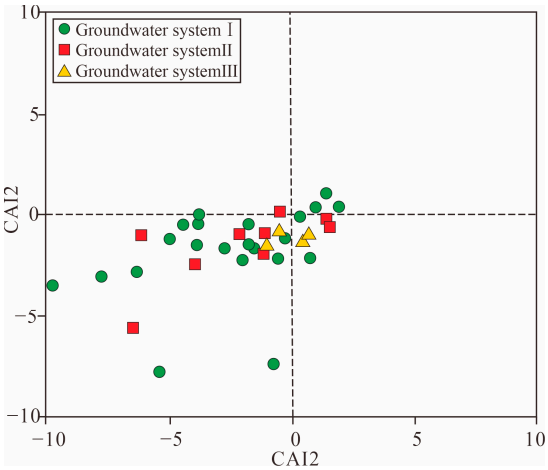

Figure 12. Chloro-alkaline indices diagram of groundwater.

3.3.4. Groundwater Saturation Index

To further understand the presence of possible mineral phases and the dissolution state in groundwater, the saturation index (SI) of minerals was calculated using PHREEQC software [39]. When SI < 0, this indicates that the mineral is in an unsaturated (dissolved)

state, while SI > 0 means that the mineral is in a saturated (precipitated) state and SI = 0 means that the aqueous solution is exactly in equilibrium with the mineral [39]. In the three groundwater systems, the average saturation indices were 0.12, 0.38, and −0.13 for calcite, 0.09, 0.49, and −0.34 for dolomite, and 0.01, 0.38, and −0.43 for aragonite, respectively, and the above minerals were basically in equilibrium in the groundwater (Figure 13). The average saturation indices of hard gypsum, gypsum, rock salt, and potassium salt in the three groundwater systems were less than 0, and the above minerals were in an unsaturated state in the groundwater. This indicates that the weathering dissolution of calcite and dolomite is the main controlling factor of the chemical composition in the groundwater, which is consistent with the results of the previous analysis.

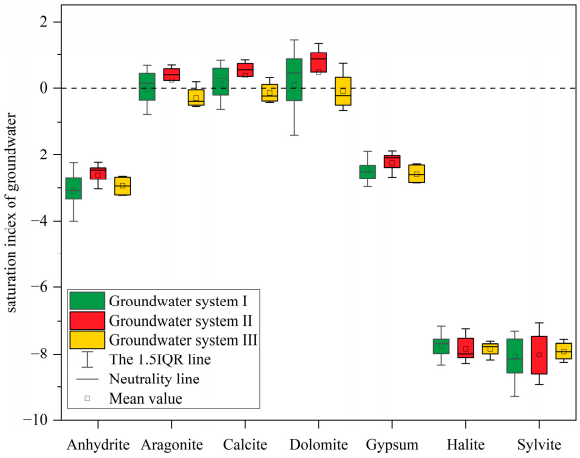

Figure 13. Box diagram of groundwater mineral saturation index in Baoshan basin.

3.4. Chemical Controlling Factors of Groundwater

The groundwater chemical characteristics of the study area are influenced by human activity factors in addition to hydrogeological conditions, water–rock interactions, and alternate cation adsorption. To further determine the degree of influence of each indicator on the chemical characteristics of the groundwater, a model was used to conduct a further analysis [40,41]. A total of fourteen indicators, including pH, K^+, Na^+, Ca^{2+}, Mg^{2+}, Cl^-, SO_4^{2-}, HCO_3^-, TDS, TH, Fe^{2+}, Mn^{2+}, NH_3-N, and COD, were selected for factor analysis considering both the detection rate and exceedance. The KMO-Bartlett sphericity test was performed for each index and the significance level was close to 0, indicating a strong correlation between the index variables that satisfied the test criteria. The Kaiser normalized maximum variance method was used to rotate the component matrix; four main factors (F1, F2, F3, and F4) were obtained, with a cumulative variance contribution of 77.84% (Table 2).

Table 2. Total variance interpretation for PCA analysis of groundwater samples.

Ingredients	Initial Eigenvalue			Extraction of the Sum of Squares of Loads			Sum of Squared Rotating Loads		
	Total	Variance (%)	Accumulation (%)	Total	Variance (%)	Accumulation (%)	Total	Variance (%)	Accumulation (%)
1	4.517	32.262	32.262	4.517	32.262	32.262	4.059	28.990	28.990
2	3.430	24.499	56.761	3.430	24.499	56.761	2.639	18.850	47.840
3	1.738	12.413	69.173	1.738	12.413	69.173	2.442	17.441	65.281
4	1.213	8.667	77.841	1.213	8.667	77.841	1.758	12.560	77.841

The main loads of dissolution filtration, migration, and enrichment factors (F1) are Ca^{2+}, Mg^{2+}, SO_4^{2-}, TDS, and TH (Table 3), with contributions of 64.56%, 84.72%, 76.14%, 86.52%, and 85.33%, respectively (Figure 14). The aquifer in the plain area has loose granular material, well-developed voids, and good runoff conditions, and the dissolution of carbonate and silicate rocks, such as tuffs, muddy tuffs, sedimentary clastic rocks, and clays, is the dominant factor in groundwater circulation. Meanwhile, the dissolution and enrichment of minerals during groundwater flow affects the changes in TDS and TH. During this process, the pore space of the aquifer is developed, the runoff is strong, the

hydraulic slope to the plain area gradually becomes slower, and the abundant carbonate rock and silicate rock minerals in the area are subject to the hydrogeochemical effect of dissolution–filtration–enrichment during the groundwater runoff process. As the local SO_4^{2-} concentration is high, there may be deep hot water recharge as well.

Table 3. Rotation factor loading matrix of groundwater indicators.

Water Chemistry Index	Ingredients			
	F1	**F2**	**F3**	**F4**
Zscore (pH)	0.273	−0.097	0.853	0.043
Zscore (Na^+)	0.036	0.818	−0.144	0.085
Zscore (K^+)	0.026	0.801	−0.326	0.061
Zscore (Ca^{2+})	0.754	0.271	0.232	−0.460
Zscore (Mg^{2+})	0.870	−0.067	0.061	−0.008
Zscore (Cl^-)	0.485	0.796	0.038	0.087
Zscore (SO_4^{2-})	0.725	−0.001	−0.139	−0.33
Zscore (HCO_3^-)	−0.178	−0.212	0.847	−0.143
Zscore (TDS)	0.977	0.087	0.025	−0.010
Zscore (TH)	0.978	0.103	0.032	−0.008
Zscore (Fe^{2+})	−0.417	0.451	0.247	0.817
Zscore (Mn^{2+})	0.043	−0.158	−0.148	0.859
Zscore (NH_3-N)	−0.216	0.556	0.103	0.720
Zscore (COD)	−0.083	0.488	−0.114	0.801

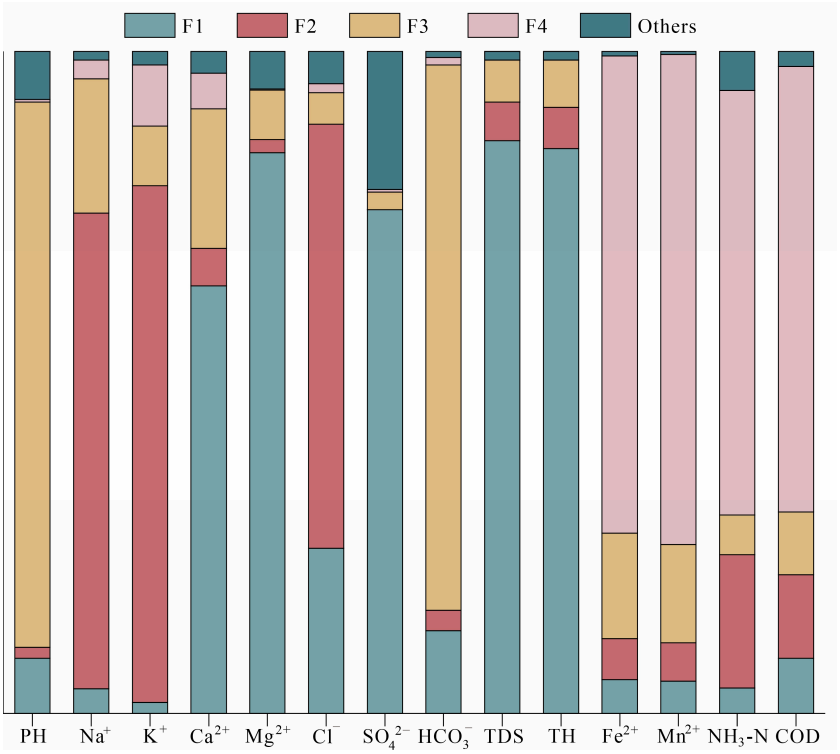

Figure 14. Contribution rate of index source for each factor.

The geological and anthropogenic factors (F2) are mainly loaded with Na^+, K^+, and Cl^- (Table 3), with contributions of 72.02%, 78.10%, and 64.19%, respectively (Figure 14). The center of the Baoshan basin is mainly deposited in the river and lake phase, and Na^+, K^+, and Cl^- are mainly derived from the cation exchange of groundwater in the basin. The center of the basin is densely inhabited and the rocks are highly permeable; thus, the groundwater is transported faster. Massive fertilization due to agriculture leads to

the transport of groundwater to the central part of the basin, while Na^+, K^+, and Cl^- in agricultural wastewater gather in the center of the basin.

The main loads of the environmental factors (F3) are pH and HCO_3^- (Table 3), with contribution rates of 82.36% and 82.38%, respectively (Figure 14). HCO_3^- in the region mainly derives from carbonate dissolution; the main lithologies in the area, such as Mawangtun in the northeastern part of the Baoshan basin and Hanzhuang in the western part, are tuffs and muddy tuffs; the groundwater runoff conditions in the pre-hill zone are strong, and carbonate weathering dissolution is strong and dominated by dissolution and filtration. Meanwhile, the shallow groundwater is mainly recharged by atmospheric precipitation, and the two together make HCO_3^- the main anion in groundwater.

The main loads of the pollution factors (F4) are Fe^{2+}, Mn^{2+}, NH_3-N, and COD (Table 3), with contributions of 72.24%, 73.44%, 64.31%, and 65.48%, respectively (Figure 14). The pleistocene quaternary in the Baoshan basin is rich in ilmenite, and the dissolution of water leads to Fe^{2+} and Mn^{2+} in the groundwater. The mineral layer contains pore pressurized water, and the top and bottom plates of the mineral layer are clay and red clay, which are poorly water-rich and have a relatively water-insulating effect, providing favorable conditions for the enrichment of Fe and Mn ions in the groundwater. The concentration of NH_3-N and COD increases due to livestock breeding, agricultural fertilization, and industrial wastewater. The high concentration of NH_3-N and COD in groundwater indicates the presence of organic matter pollution, and ammonia nitrogen dissolves in water, making the groundwater environment reductive, which in turn reduces the material in titaniferous sand ore to divalent free state Fe and Mn, causing the concentration of Fe^{2+} and Mn^{2+} in groundwater to increase.

4. Conclusions

Shallow groundwater chanting of the quaternary is widely used in the production and life of the inhabitants of the Baoshan basin. In this paper, the chemical evolution of groundwater and the causes of water contamination in the Baoshan basin are discussed using mathematical and statistical methods, the TIS diagram, Piper's trilinear diagram, Gibbs plots, the Gaillardet model, the ion scale factor, the saturation index, and the PCA-APCS-MLR model. The following conclusions can be drawn.

(1) The geochemical type of the shallow groundwater of the quaternary in the Baoshan basin is dominated by HCO_3-Ca-Mg and HCO_3-Ca. The main cations are Ca^{2+}, Na^+, and Mg^{2+}, and the main anions are HCO_3^- and Cl^-, among which Ca_{2+}, Na_+, and HCO_3^- have a high contribution to TDS, which is consistent with the results of the statistical eigenvalue analysis of water chemistry parameters. The total salinity (TIS) corroborates that HCO_3^- is the main anion in the region. Fe^{2+}, Mn^{2+}, and NH_3-N have variation coefficients greater than 1 in groundwater systems I and II, and are the main pollutants in the groundwater of the Baoshan basin.

(2) The genesis of water chemical characteristics is mainly influenced by water–rock interaction. The types of rocks with which material exchange with groundwater occurs are carbonate rocks (limestones, argillaceous limestones, red clay) and silicate rocks (sandstone, shale, clay), which are the main sources controlling Ca^{2+}, Mg^{2+}, SO_4^{2-}, and HCO_3^- in the groundwater of the Baoshan basin. Na^+, K^+, and Cl^- in groundwater mainly originate from alternate cation adsorption, and agricultural pollution is an important source as well. According to the results of the PHREEQC softwares calculation of groundwater mineral saturation, it is clear that the weathering dissolution of calcite and dolomite is the main controlling factor of chemical composition in the groundwater, which is consistent with the results of the previous analysis.

(3) Based on the calculation results of the PCA-APCS-MLR model, four main factors were obtained, namely, dissolved filtration, migration, and enrichment (F1), geological and human activity (F2), environmental factors (F3), and pollution factors (F4), with a cumulative variance contribution of 77.84%. F1 was mainly loaded with Ca^{2+},

Mg^{2+}, $SO_4{}^{2-}$, TDS, and TH; for F2, the main loads were Na^+, K^+, and Cl^-; for F3, the main loads were pH and $HCO_3{}^-$; and for F4, the main loads were Fe^{2+}, Mn^{2+}, NH_3-N, and COD. Pollution due to Fe^{2+} and Mn^{2+} mainly derives from the groundwater dissolved filtration of titaniferous sand ore in the quaternary strata and industrial wastewater discharge, while NH_3-N pollution mainly derives from the direct discharge of domestic and agricultural wastewater.

In view of the current situation that Fe^{2+}, Mn^{2+}, and NH_3-N exceed standards in the shallow groundwater of the quaternary in the Baoshan basin, the spatial distribution characteristics and migration pattern of pollutants should be further studied. Industrial wastewater and agricultural wastewater should be discharged after reaching the standards to prevent further pollution of the groundwater.

Author Contributions: Conceptualization, S.X.; methodology, T.G.; software, Y.X. and J.Z.; validation, S.X.; formal analysis, J.Z.; investigation, Y.X. and J.Z.; resources, A.L. and S.X.; data curation, Y.X.; writing—original draft preparation, Y.X.; writing—review and editing, A.L. and X.G.; visualization, J.Z.; supervision, X.D. and P.Z.; project administration, A.L.; funding acquisition, A.L. All authors have read and agreed to the published version of the manuscript.

Funding: This work was supported by the "Ten Thousand People Plan" of China for Science and Technology Innovation Leaders and the National Natural Science Foundation of China (Grant No. 52179028).

Data Availability Statement: The data presented in this study are available on request from the corresponding author.

Acknowledgments: The authors thank Yanhua Zhang, Jianhua Chai, Hongyi Fu, and Songtao Han for their fieldwork support. At the same time, the reviewers gave a lot of constructive comments. The editors were very efficient in handling the manuscript throughout the process. We would like to express our gratitude here.

Conflicts of Interest: The authors declare no conflict of interest.

References

1. Habibah, A.A.; Dahab, K.; Shabana, A.; Kamh, S.; Ibrahim, H. Assessment of the Hydrogeochemical Characteristics of Groundwater Resources at some Wadis in the East of El Minia Governorate, Eastern Desert, Egypt. *J. Acta Geol. Sin.* **2022**, *96*, 1082–1097. [CrossRef]
2. Gao, Y.; Chen, J.; Qian, H.; Wang, H.; Ren, W.; Qu, W. Hydrogeochemical characteristics and processes of groundwater in an over 2260 year irrigation district: A comparison between irrigated and nonirrigated areas. *J. Hydrol.* **2022**, *606*, 127437. [CrossRef]
3. Jabbo, J.N.; Isa, N.M.; Aris, A.Z.; Ramli, M.F.; Abubakar, M.B. Geochemometric approach to groundwater quality and health risk assessment of heavy metals of Yankari Game Reserve and its environs, Northeast Nigeria. *J. Clean. Prod.* **2022**, *330*, 129916. [CrossRef]
4. Jha, S.K.; Mishra, V.K.; Verma, C.L.; Sharma, N.; Sharma, B.R. Groundwater quality concern for wider adaptability of novel modes of managed aquifer recharge (MAR) in the Ganges Basin, India. *Agric. Water Manag.* **2021**, *246*, 106659. [CrossRef]
5. Takaya, K. Long-Term Reaction Characteristics of CO_2-Water-Rock Interaction: Insight into the Potential Groundwater Contamination Risk from Underground CO_2 Storage. *Resour. Geol.* **2018**, *68*, 93–100. [CrossRef]
6. Abdelgawad, A.M.; Watanabe, K.; Takeuchi, S. Water-rock interaction study on the occurrence of fluoride-rich groundwater at Mizunami area, Japan. *Environmentasia* **2009**, *2*, 20–29.
7. Jiang, J.; Fu, G.; Feng, Y.; Gu, X.; Jiang, P.; Shen, C.; Chen, Z. Characteristics and Causes of Coastal Water Chemistry in Qionghai City, China. *Appl. Sci.* **2023**, *13*, 5579. [CrossRef]
8. Chen, L.; Wang, G.; Hu, F.; Wang, Y.; Liu, L. Groundwater hydrochemistry and isotope geochemistry in the Turpan Basin, northwestern China. *J. Arid Land* **2014**, *6*, 378–388. [CrossRef]
9. Soboleva, E.B.; Tsypkin, G.G. Regimes of haline convection during the evaporation of groundwater containing a dissolved admixture. *Fluid Dyn.* **2016**, *51*, 364–371. [CrossRef]
10. Meredith, K.T.; Hollins, S.E.; Hughes, C.E.; Cendón, D.I.; Chisari, R.; Griffiths, A.; Crawford, J. Evaporation and concentration gradients created by episodic river recharge in a semi-arid zone aquifer: Insights from Cl−, δ18O, δ2H, and 3H. *J. Hydrol.* **2015**, *529*, 1070–1078. [CrossRef]
11. Kim, K.; Yun, S.T. Buffering of sodium concentration by cation exchange in the groundwater system of a sandy aquifer. *Geochem. J.* **2005**, *39*, 273–284. [CrossRef]

12. Xing, L.; Gao, H.; Zhan, Y. Groundwater hydrochemical characteristics and processes along flow paths in the North China Plain. *J. Asian Earth Sci.* **2013**, *S70–S71*, 250–264. [CrossRef]
13. Liu, Y.; Zhou, X.; Deng, Z.; Fang, B.; Tsutomu, Y.; Zhao, J.; Wang, X. Hydrochemical characteristics and genesis analysis of the Jifei hot spring in Yunnan, southwestern China. *Geothermics* **2015**, *53*, 38–45. [CrossRef]
14. Tian, X.; Fei, Y.-H.; Zhang, J.-L.; Li, Y.-S.; Dun, Y.; Guo, C.-Y. Analysis on hydrochemical characteristics of groundwater in strongly exploited area in Hutuo River Plain. *J. Groundw. Sci. Eng.* **2017**, *2*, 44–53.
15. Nathaniel, A.; Abigail, A. Comparative Analysis of the Hydrochemical Characteristics of Ground Water Sources Found within the Kassena Nankana East District of the Upper East Region of Ghana. *Am. J. Min. Met.* **2017**, *4*, 45–50.
16. Chotpantarat, S.; Thamrongsrisakul, J. Natural and anthropogenic factors influencing hydrochemical characteristics and heavy metals in groundwater surrounding a gold mine, Thailand. *J. Asian Earth Sci.* **2021**, *211*, 104692. [CrossRef]
17. Li, J.; Wang, W.; Wang, D.; Li, J.; Dong, J. Hydrochemical and Stable Isotope Characteristics of Lake Water and Groundwater in the Beiluhe Basin, Qinghai—Tibet Plateau. *Water* **2020**, *12*, 2269. [CrossRef]
18. Sivasubramanian, P.; Balasubramanian, N. Hydrochemical characteristics of coastal aquifers of Kadaladi, Ramanathapuram District, Tamilnadu, India. *Appl. Water Sci.* **2013**, *3*, 603–612. [CrossRef]
19. Pazand, K.; Khosravi, D.; Ghaderi, M.R.; Rezvaniyanzadeh, M.R. Identification of the hydrogeochemical processes and assessment of groundwater in a semi-arid region using major ion chemistry: A case study of Ardestan basin in Central Iran. *Groundw. Sustain. Dev.* **2018**, *6*, 245–254. [CrossRef]
20. Bouri, S.; Nsiri, M.; Brahim, F.B.; Khlifi, M. Assessment of the effects of anthropogenic activities on the El Arich groundwater using hydrogeochemistry, GIS and multivariate statistical techniques: A case study of the semi-arid Kasserine region, Tunisia. *Environ. Qual. Manag.* **2022**, *31*, 261–281.
21. Ren, K. Effects of Urbanization on Groundwater Quality of Laolongdong Watershed. In Proceedings of the First Joint Scientific Meeting of Geological Society of China (GS) Cand Geological Society of America (GSA) (Roof of the World), Chengdu, China, 17–19 June 2013; Volume 87, pp. 384–398.
22. Karunanidhi, D.; Subramani, T.; Roy, P.D.; Li, H. Impact of groundwater contamination on human health. *Environ. Geochem. Health* **2021**, *43*, 643–647. [CrossRef] [PubMed]
23. Meng, L.; Zuo, R.; Wang, J.S.; Yang, J.; Shi, R.T. Quantitative source apportionment of groundwater pollution based on PCA-APCS-MLR. *China Environ. Sci.* **2017**, *37*, 3773–3786.
24. Zhang, H.; Cheng, S.; Li, H.; Fu, K.; Xu, Y. Groundwater pollution source identification and apportionment using PMF and PCA-APCA-MLR receptor models in a typical mixed land-use area in Southwestern China. *Sci. Total Environ.* **2020**, *741*, 140383. [CrossRef]
25. Xiao, Y.; Zhang, J.; Guo, T. Evaluation of Quaternary Groundwater Quality Based on AHP-Entropy Weight Method in Baoshan Basin, Yunnan, China. *World Sci. Res. J.* **2021**, *7*, 76–82.
26. He, Y.; Li, N.; Wang, Z.; Wang, H.; Yang, G.; Xiao, L.; Wu, J.; Sun, B. Quercus yangyiensis sp. nov. from the late Pliocene of Baoshan, Yunnan and its paleoclimatic significance. *Acta Geol. Sin.* **2014**, *88*, 738–747. [CrossRef]
27. Yu, Y.; Wang, J.; Cheng, F.; Deng, H.; Chen, S. Drought monitoring in Yunnan Province based on a TRMM precipitation product. *Nat. Hazards* **2020**, *104*, 2369–2387. [CrossRef]
28. Bao, Z.Y. Hydrogeological Conditions and Searching for Groundwater in the Baoshan Region, Yunnan. *Acta Geol. Sichuan* **2012**, *32*, 87–91.
29. Han, Z.; Xiang, H.; Guo, S. Sinistral shear and extension of the northern section of Lijiang Basin in northwest Yunnan in Quaternary. *Chin. Sci. Bull.* **2005**, *50*, 452–459. [CrossRef]
30. Dai, S.; Liu, S.; Zhao, Y.; Zhao, Z.; Gao, F.; Wu, S.; Mou, F. The Formation and Evolution of the Baoshan Basin, Yunnan Province. *Pet. Geol. Exp.* **1998**, *S1*, 178–180.
31. Huang, H.; Liu, L. An Application of EVS Hybrid Modeling Method. *Soil Eng. Found.* **2022**, *36*, 208.
32. Green, C.T.; Bekins, B.A.; Kalkhoff, S.J.; Hirsch, R.M.; Liao, L.; Barnes, K.K. Decadal surface water quality trends under variable climate, land use, and hydrogeochemical setting in Iowa, USA. *Water Resour. Res.* **2014**, *50*, 2425–2443. [CrossRef]
33. Hoaghia, M.-A.; Roman, C.; Tanaselia, C.; Ristoiu, D. Groundwater chemistry rendering using Durov, Piper and ion balance diagrams. Study case: The northern part of Sibiu county. *Sud. Univ. Babeș-Bolyai Chem.* **2015**, *2*, 161–168.
34. Apollaro, C.; Tripodi, V.; Vespasiano, G.; De Rosa, R.; Dotsika, E.; Fuoco, I.; Critelli, S.; Muto, F.J.M.; Geology, P. Chemical, isotopic and geotectonic relations of the warm and cold waters of the Galatro and Antonimina thermal areas, southern Calabria, Italy. *Mar. Pet. Greol.* **2019**, *109*, 469–483. [CrossRef]
35. Marandi, A.; Shand, P. Groundwater chemistry and the Gibbs Diagram. *Appl. Geochem.* **2018**, *97*, 209–212. [CrossRef]
36. Wu, C.; Wu, X.; Lu, C.; Sun, Q.; He, X.; Yan, L.; Qin, T. Hydrogeochemical characterization and its seasonal changes of groundwater based on self-organizing maps. *Water* **2021**, *13*, 3065. [CrossRef]
37. Elumalai, V.; Rajmohan, N.; Sithole, B.; Li, P.; Uthandi, S.; van Tol, J. Geochemical evolution and the processes controlling groundwater chemistry using ionic ratios, geochemical modelling and chemometric analysis in uMhlathuze catchment, KwaZulu-Natal, South Africa. *Chemosphere* **2023**, *312*, 137179. [CrossRef]
38. Zhang, J.; Shi, Z.; Wang, G.; Jiang, J.; Yang, B. Hydrochemical characteristics and evolution of groundwater in the Dachaidan area, Qaidam Basin. *Earth Sci. Front.* **2021**, *28*, 194.

39. Apollaro, C.; Marini, L.; De Rosa, R. Use of reaction path modeling to predict the chemistry of stream water and groundwater: A case study from the Fiume Grande valley (Calabria, Italy). *Environ. Geol.* **2007**, *51*, 1133–1145. [CrossRef]
40. Li, W.; Wu, J.; Zhou, C.; Nsabimana, A. Groundwater pollution source identification and apportionment using PMF and PCA-APCS-MLR receptor models in Tongchuan City, China. *Arch. Environ. Contam. Toxicol.* **2021**, *81*, 397–413. [CrossRef]
41. Meng, L.; Zuo, R.; Wang, J.-S.; Yang, J.; Teng, Y.-G.; Shi, R.-T.; Zhai, Y.-Z. Apportionment and evolution of pollution sources in a typical riverside groundwater resource area using PCA-APCS-MLR model. *J. Contam. Hydrol.* **2018**, *218*, 70–83. [CrossRef]